Synergistic Fusion of Interferometric and Speckle-Tracking Methods for Deriving Surface Velocity From Interferometric SAR Data

Hongxing Liu, *Member, IEEE*, Zhiyuan Zhao, and Kenneth C. Jezek, *Associate Member, IEEE*

Abstract—This letter presents a technique to adjust and unify disconnected interferogram fringe regions for the derivation of accurate surface-velocity measurements. The interferogram from repeat-pass interferometric synthetic aperture radar data is often partitioned by shear margins of ice streams and other low-coherence zones into many small disconnected fringe regions. Although these isolated fringe regions can be unwrapped separately, the unwrapped phase for each region is referenced to a different seed point. Our technique exploits absolute range-offset measurements from the speckle-tracking method to bridge the isolated fringe regions in the interferogram. In this way, the unwrapped phases in these regions can be adjusted into consistent surface-displacement measurements with a common reference point. Using Radarsat interferometric data in Antarctica, we demonstrated that the synergetic fusion of the measurements from the interferometric and speckle-tracking methods can produce a highly accurate two-dimensional velocity field.

Index Terms—Data fusion, fringe regions, interferometric synthetic aperture radar (InSAR), phase unwrapping, speckle tracking.

I. INTRODUCTION

ICE VELOCITY measurements are fundamentally important in studying glacial flow dynamics and ice-sheet mass balance [1]–[3]. The repeat-pass interferometric data acquired by synthetic aperture radar (SAR) sensors onboard the European Remote Sensing 1 (ERS-1) and 2 (ERS-2) and Radarsat satellites have been widely used to measure surface-motion speeds and directions [4]–[6]. The phase-unwrapping-based interferometric method [7] and speckle-tracking method [1], [2], [6] have been established as two complementary approaches to processing repeat-pass interferometric data. Recently, Joughin [6] demonstrated that velocity measurements in the range direction derived from the conventional interferometric method can be combined with velocity measurements in the azimuth direction derived from speckle-tracking methods to create a two-dimensional (2-D) velocity field. However, in previous studies, the interferograms are assumed to be continuous. In reality, the

interferogram from repeat-pass interferometric SAR (InSAR) data is often partitioned by shear margins of ice streams and other low-coherence zones into disconnected fringe regions. Although various phase-unwrapping algorithms have been developed, these algorithms can only unwrap the isolated fringe regions separately, with different reference (seed) points. To utilize the fragmented phase information, these fringe regions need to be linked and adjusted with a common reference point. Joughin [6] mentioned the possibility of utilizing speckle-tracked range offset to remove the ambiguities of relative phase offsets between separate fringe regions.

In this letter, we present a novel technique to unify the unwrapped phases in the disconnected fringe regions with a common reference point. This technique exploits absolute range-offset measurements from the speckle-tracking method to bridge the isolated fringe regions in an interferogram. Using Radarsat InSAR data for Antarctica, we demonstrate that the range displacement measurements from the interferometric method and the azimuth displacement measurements from the speckle-tracking method can be fused to produce a precise 2-D velocity field.

II. PHASE UNWRAPPING AND SPECKLE TRACKING

A SAR sensor measures both radar backscattering information and distance information for ground features. The distance information is encoded in phase. The phase differences in the two complex SAR images acquired during repeat passes, known as an interferogram, can be calculated by subtracting the phase in one image from the phase in the other. The phase values in the interferogram wrap around in cycles of 2π, and the ambiguity of the correct multiple of 2π needs to be resolved for the absolute surface-displacement measurements in the radar line-of-sight (LOS) direction. Various phase-unwrapping algorithms have been developed in the past decades [7]–[10]. The phase measurement in the interferogram includes contributions from baseline, topography, and surface-motion effects. The baseline effect, namely, the flat terrain phase ramp, can be removed with knowledge of SAR imaging geometry to generate a flattened (deramped) interferogram. The topography effect can be further removed from the flattened interferogram by using a digital elevation model or using a double-difference technique when more than two passes of SAR data are available [5]. After the removal of the baseline and topography effects, the phase values in the interferogram are proportional to surface
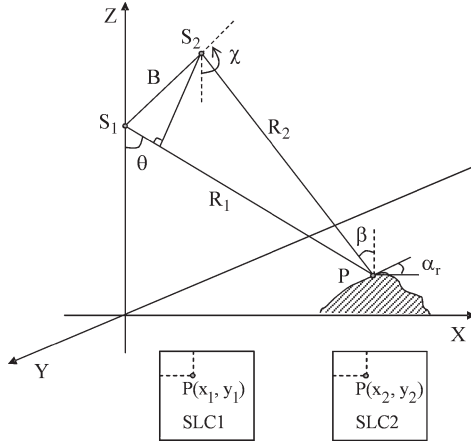
Fig. 1.   Geometry of repeat-pass interferometry.

displacements in the LOS direction. To obtain the absolute surface-motion measurements, an unknown constant phase, associated with the arbitrary selection of initial seed point for phase unwrapping, needs to be determined [2]

$$\Phi_m = \Phi - \Phi_0 \tag{1}$$

where Φ_m is the surface-motion-induced phase in the LOS direction, Φ is the unwrapped phase after the removal of baseline and topography effects, and Φ_0 is the unknown constant phase to be solved.

Under the assumption that the ice flow vector is parallel to the ice surface, the radial LOS velocity can be projected into local horizontal surface velocities in the range direction [5]

$$V_r = \frac{\lambda}{4\pi T \sin(\beta + \alpha_r)} \Phi_m \tag{2}$$

where V_r is the surface-motion velocity in the range direction, λ is the wavelength of the radar signal in meters, T is the time interval between acquisitions, β is the incidence angle, and α_r is the surface slope angle in the range direction. The geometry parameters of interferometry are illustrated in Fig. 1.

The speckle-tracking method has been developed as an alternative approach to the processing of repeat-pass InSAR data for surface velocity [1], [2], [6]. A correlation-matching algorithm is commonly used to obtain both azimuth and range-direction offsets based on the coherent speckle pattern of small chips of two repeat-pass SAR image acquisitions [1], [2], [6]. Through oversampling of the correlation surface, the matching peak can be determined to a small fraction of a pixel. The range offset δ_r and azimuth offset δ_a detected from cross-correlation matching include a nonmotion component contributed by the imaging geometry (baseline effect and orbital crossing) and topography effect. The topography-induced offsets only occur in the range direction and can be removed by using a digital elevation model. The geometry-induced terms in the range and azimuth offset can be modeled and removed using two linear equations

$$d_r = \delta_r - (a_0 + a_1 x + a_2 y) \tag{3}$$
$$d_a = \delta_a - (b_0 + b_1 x + b_2 y) \tag{4}$$

where d_r and d_a are, respectively, the surface displacements in the range and azimuth directions measured in pixels, x and y are the range and azimuth coordinates of the slant range image, a_0, a_1, and a_2 are coefficients for accounting for the geometry term in range direction, and b_0, b_1, and b_2 are coefficients for accounting for the geometry term in the azimuth direction. The velocity components in range (V_r) and azimuth (V_a) directions can be calculated from

$$V_r = \frac{d_r - B\cos(\chi - \theta)}{T\sin(\beta + \alpha_r)} \cdot S_r \tag{5}$$

$$V_a = \frac{d_a}{T\cos(\alpha_a)} \cdot S_a \tag{6}$$

where B is the length of the baseline (converted to unit in range pixel), χ is the baseline angle, θ is the radar look angle, α_a is the terrain slope in the azimuth directions, and S_r and S_a are pixel sizes in meters in range and azimuth directions.

Two-dimensional surface-motion speed (s) and direction (ψ) can be calculated by the following equations:

$$s = \sqrt{V_r^2 + V_a^2} \tag{7}$$

$$\psi = \arctan\left(\frac{V_a}{V_r}\right). \tag{8}$$

The conventional interferometric method and speckle-tracking method have their advantages and limitations [1], [2], [6]. The major advantage of the interferometric method is that surface-displacement measurements in the range direction have an intrinsically high accuracy at a fraction of the radar signal wavelength. However, in fast-moving areas, the high fringe rate of the interferogram may make the phase unwrapping impossible. The shear margins of the ice streams and outlet glaciers and other low-coherence zones induced by radar shadows, layover, and temporal decorrelation often fragment the interferogram into many small disconnected fringe regions. Since the speckle-tracking method is less sensitive to decorrelation and does not require phase unwrapping, it is able to provide displacement measurements farther into the shear margins and across areas with a high moving velocity. Furthermore, with a single InSAR image pair, the speckle-tracking method can derive surface displacements in both range and azimuth directions, in contrast to the range-only displacement measurements of the conventional interferometric method. To make full use of the comparative advantages of both methods, the range motion component derived from the interferometric method and the azimuth motion component derived from the speckle-matching method should be combined whenever possible [1], [2], [6].

III. LINKING DISCONNECTED FRINGE REGIONS

For an interferometric data pair, assume that the interferogram is partitioned into m fringe regions by highly decorrelated zones. Each fringe region can be individually unwrapped by selecting a seed point inside each region. As shown in (1), each fringe region has an unknown parameter Φ_0, corresponding to its own reference seed point. There are m unknowns in total for the entire image.

The mathematical relationship between the phase measurement and the range-offset measurement for the same pixel can be derived from the geometry of repeat-pass interferometry. The ranges R_1 and R_2 from the SAR sensor to the point P in the first and second passes (Fig. 1) can be expressed as linear functions of the slant range coordinates of the pixel in single-look complex (SLC) images

$$R_1 = R_1^0 + x_1 S_r \qquad (9)$$
$$R_2 = R_2^0 + x_2 S_r \qquad (10)$$

where x_1 and x_2 are the slant range coordinates of the pixel in the first and the second images. R_1^0 and R_2^0 are ranges from the SAR sensor to the first pixel in the first and second images. S_r is the pixel size in the range direction. The range difference ΔR can be calculated by

$$\Delta R = R_2 - R_1 = \left(R_2^0 - R_1^0\right) + S_r \delta_r \qquad (11)$$

where $\delta_r = x_2 - x_1$ is the range offset of the pixel measured by the speckle-tracking method. For any pixel in fringe region i, the range difference ΔR can be correlated to its unwrapped phase Φ by

$$\Delta R = \frac{\lambda}{4\pi}\left(\Phi - \Phi_0^i\right) \qquad (i=1,\ldots,m) \qquad (12)$$

where Φ_0^i is a constant unknown value for fringe region i associated with the selected reference seed point in the phase unwrapping. Combing (11) and (12), we obtain

$$\Phi_0^i = \frac{4\pi}{\lambda}\left(R_2^0 - R_1^0\right) + \left(\Phi - \frac{4\pi}{\lambda}S_r\delta_r\right) \qquad (i=1,\ldots,m). \quad (13)$$

In (13), R_1^0, R_2^0, and S_r are constant values for SAR images, the unwrapped phase Φ is a relative measurement in unit of radians with respect to an arbitrary reference point, and the range offset δ_r is an absolute measurement in unit of pixels across the entire image frame. Both the unwrapped phase Φ and the range offset δ_r contain the combined effects of the baseline, topography, and surface motion. Using the SAR imaging geometry and a digital elevation model, the baseline and topography effects can be removed from the phase and range-offset measurements. After the removal, (13) is still valid since the baseline and topography effects in the phase and the range-offset measurements are canceled in the right side of the equation. Because baseline and topography effects cause phase ramp and a high fringe rate in the interferogram, it is a common practice to remove both baseline and topography effects in (13) to facilitate the phase-unwrapping operation.

Assume that there are N pixels in the fringe region i; then we can obtain N observation equations by inserting the unwrapped phase and range-offset measurements for each pixel into (13). By minimizing the sum of squared deviations between the adjusted phases and absolute range-offset measurements for all pixels in the fringe region, we derive an optimal estimate for the unknown constant phase parameter $(\hat{\Phi}_0^i)$ for the fringe region i

with the least square criterion. It is given by the following equation:

$$\hat{\Phi}_0^i = \frac{4\pi}{\lambda}\left(R_2^0 - R_1^0\right) + \frac{1}{N}\sum_{j=1}^{N}\left(\Phi^j - \frac{4\pi}{\lambda}S_r\delta_r^j\right)$$
$$(i=1,\ldots,m) \qquad (14)$$

where Φ^j and δ_r^j are, respectively, the unwrapped phase and range-offset measurements for pixel $j(j=1,\ldots,N)$ in the fringe region i.

The estimate error in Φ_0^i can be quantified by the following formula:

$$\sigma_{\Phi_0^i}^2 = \frac{1}{N}\sigma_\Phi^2 + \frac{16\pi^2 S_r^2}{N\lambda^2}\sigma_\delta^2 = \frac{1-\gamma^2}{2NM_1\gamma^2} + \frac{24S_r^2(1-\gamma^2)}{NM_2\lambda^2\gamma^2} \quad (15)$$

where σ_δ is the range-offset measurement error from the speckle-tracking method, and σ_Φ is the phase measurement error from the interferometric method. These two error terms are further expanded in (15) using the error equations provided in [11]. γ is the coherence level, M_1 is the number of independent pixels in the forming multilook interferogram, and M_2 is the number of pixels within the correlation window in the speckle-tracking method. $\sigma_{\Phi_0^i}^2$ is a systematic error for fringe region i introduced in the cross-region phase adjustment. It is inversely proportional to N, which is the number of pixels in the fringe region.

Equation (14) gives an optimal estimate for the unknown constant phase term Φ_0^i for each fringe region based on the absolute range-offset measurements from the speckle-tracking method. By subtracting the optimally estimated constant phase term from the original unwrapped phase measurements for each fringe region, we obtain the adjusted phase values. After the phase adjustment, all fragmented fringe regions are unified, in the sense that they have accurate absolute phase measurements relative to a common reference.

IV. SYNERGISTIC FUSION

An InSAR data pair over the Recovery Glacier, Antarctica, is used to demonstrate our data fusion technique. The two SAR images in the interferometric pair were acquired on September 21 and October 15, 1997 by the Radarsat-1 SAR sensor with the standard beam 7. The parallel baseline is 206.3 m, and the perpendicular baseline is 215.8 m. In the scene, the tributary RAMP glacier flows from the top and merges into the Recovery Glacier, which moves from the left to the right [Fig. 2(a)]. High backscatter returns are apparent in the shear margins of both the Recovery and the RAMP glaciers. The SLC images were coregistered at subpixel accuracy, and the level of coherence between the SLC image was calculated [Fig. 2(b)]. Due to high deformations and ice crevasses, shear margins of the glaciers exhibit a very low coherence and appear in dark tone. With coregistered SLC images, the interferogram was calculated. With knowledge of the SAR imaging geometry and a digital elevation model [12], the effects of the baseline and topography were removed, resulting in a motion-only interferogram (Fig. 3). Clearly, the areas of slowly moving ice sheet denoted by A and B and the glacial floors
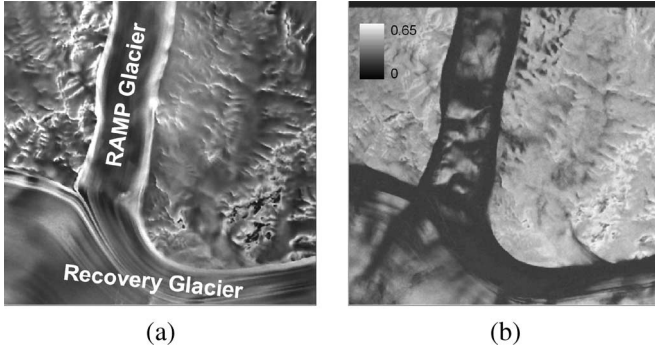
Fig. 2. Interferometric data over the Recovery Glacier, Antarctica. (a) SAR intensity image (3550 × 2593 pixels). (b) Coherence image (3550 × 2593 pixels).

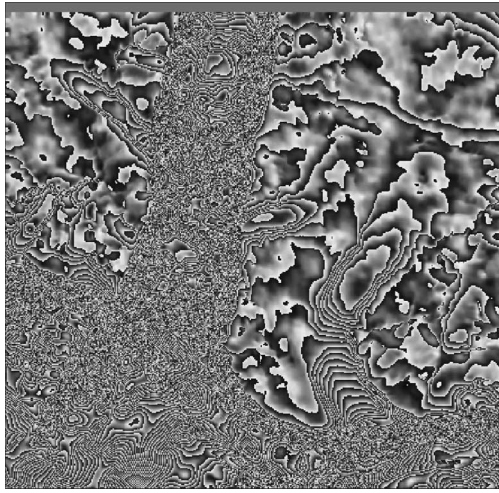Fig. 3. Interferogram after removal of baseline and topography effects.
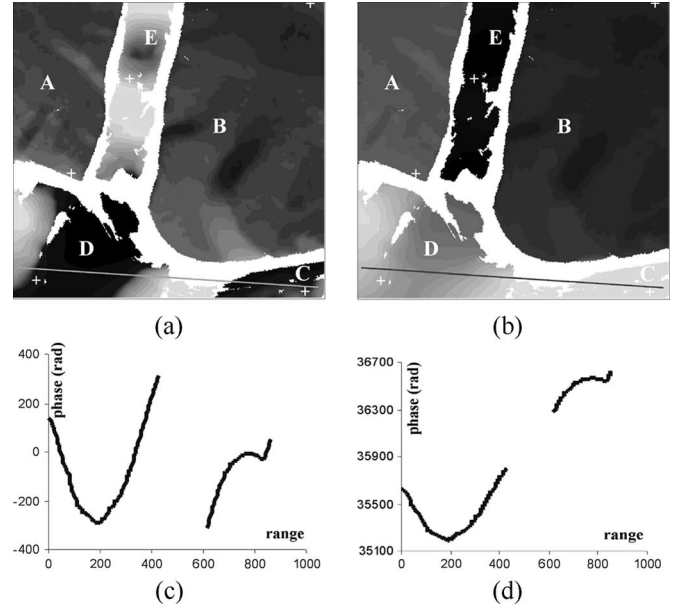

Fig. 4. Cross-region phase adjustment for five isolated fringe regions. (a) Unwrapped phase before adjustment. (b) Unwrapped phase after adjustment. (c) Phase profile before adjustment. (d) Phase profile after adjustment. The plus signs in (a) and (b) indicate the locations of seed points, and lines indicate the position of profiles.

TABLE I
STATISTICS OF PHASE-ADJUSTMENT CROSS FRINGE REGIONS

Region	Seed Point	N	Φ_0^i (rad)	σ_{Φ_0}(rad)
A	200, 200	1994	17471	0.8
B	2500, 1000	5172^2	17318	0.5
C	3363, 2545	287	20091	2.1
D	70, 2500	1607	19007	0.9
E	1420, 500	884	16559	1.2

(denoted by C, D, and E) between shear margins have quite sharp fringes. The five fringe regions A, B, C, D, and E are spatially separated by highly decorrelated shear margins, where the fringe pattern was completely destroyed and invisible.

By using the branch-cut algorithm [7], the five fringe regions were separately unwrapped with five arbitrarily selected seed reference points [Fig. 4(a)]. The location of the seed point for each fringe region is shown in Fig. 4.

Using the speckle-tracking method, we computed range offsets. Then, the topography- and geometry-induced components in the range offsets are removed. With the motion-only phase and motion-only range-offset measurements, we calibrated the unknown constant phase parameter $\Phi_0^i (i = 1, \ldots, 5)$ for each fringe region using (14). The estimation error for the parameter (Table I) is also computed by using (15), in which $S_r = 8.1$ m, $\sigma_\delta = 0.02$ pixels, and $\sigma_\Phi = 0.2$ rad. σ_δ and σ_Φ are estimated by the equations in [11]. As shown in Table I, the estimation error is very small. For fringe region C, 2.1-rad error in Φ_0^i is equivalent to a velocity error of 0.14 m/year.

The unified absolute phase is shown in Fig. 4(b). Now, the phase measurements of the spatially disconnected fringe regions have been adjusted to a common reference point and hence are consistent and comparable. Fig. 4(c) and (d) shows the phase profiles before and after the phase adjustment. The profile horizontally crosses through fringe regions D and C.

Before the phase adjustment, there is a steep discontinuity between two segments of unwrapped phase from regions D and C. After the phase adjustment, the two segments of phase measurements are well aligned up.

The adjusted phase measurements are further converted into the range velocity by using (2). The range-velocity gaps between the fringe regions are filled up by the less accurate range-offset measurements from the speckle-tracking method through (5). The speckle-tracking method provides displacement measurements farther into the shear margins and areas of high strain rate, because it is less sensitive to decorrelation than the phase-unwrapping method.

We also computed the azimuth offsets by using the speckle-tracking method. The azimuth offset measurements are significantly more accurate than range-offset measurements for the speckle-tracking method. This is mainly because the azimuth resolution (about 5.4 m) is much better than the range resolution (about 8.1 m) in the SLC images. The geometry effect in the derived azimuth offsets is modeled and removed using (4). The motion-only azimuth offsets are further converted into azimuth velocity measurements using (6). By combining the range and azimuth velocity components through (7) and (8), we derive the ice flow speed and direction in 2-D space (Fig. 5).

Clearly, the derived flow directions agree well with the flow stripes observed from the SAR image. The spatial pattern of
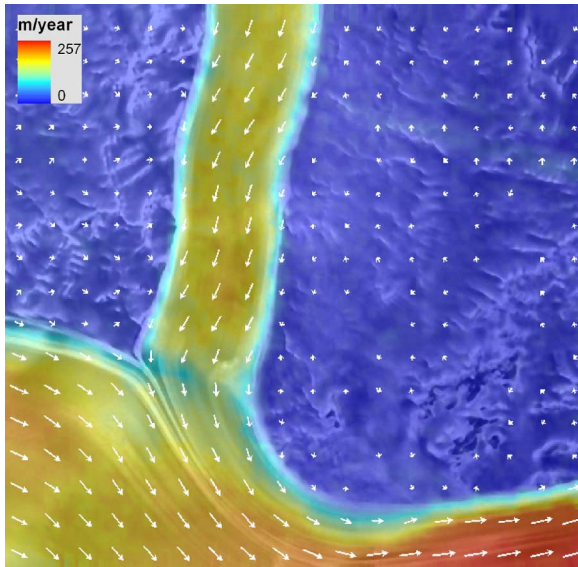
Fig. 5. Two-dimensional velocity field produced by fusing phase unwrapping and speckle-tracking measurements.

speed variation is consistent with the glacial features and the topography. The glacial channels have the fastest flow speed, up to 257 m/year. The flow velocity decreases in the junction region where the tributary RAMP glacier merges into the main Recovery Glacier [2]. By comparing with ice flow stripes and independent velocity measurements, the derived flow directions are evaluated to be accurate within $5°$, and the flow speeds are accurate to about 10–15 m/year [2]. No obvious artifacts from atmospheric effects [1] have been detected in our interferometric data set.

V. CONCLUSION

We developed a technique to adjust and correlate the disconnected fringe regions in an interferogram by utilizing the absolute range-offset measurements from the speckle-tracking method. Our technique is particularly useful for the areas with a high motion speed and for InSAR data pairs with a long temporal baseline like Radarsat data, in which the shear margins of fast-moving glaciers and ice streams and other temporally decorrelated channels often partition the interferogram into isolated fringe regions. An alternative method to adjust disconnected fringe regions is to identify one or more velocity control points for each fringe region. However, velocity control points are frequently not available for all segmented regions. For our application example, we can use exposed rocks in fringe regions A and B as zero-velocity control points, but no velocity control points can be identified for fringe regions C, D, and E. In this sense, our technique greatly reduces the demands for velocity control points. The surface-displacement measurements derived from the conventional interferometric method and speckle-tracking method are complementary. Our application example demonstrates that the synergistic fusion of measurements from the phase-unwrapping-based interferometric method and speckle-tracking method spawns a highly accurate 2-D velocity field with a single interferometric data pair.

REFERENCES

[1] A. L. Gray, N. Short, K. E. Matter, and K. C. Jezek, "Velocities and ice flux of the Filchner ice shelf and its tributaries determined from speckle tracking interferometry," *Can. J. Remote Sens.*, vol. 27, no. 3, pp. 193–206, Jun. 2001.

[2] Z. Zhao, "Surface velocities of the East Antarctic ice streams from Radarsat-1 interferometric synthetic aperture radar data," Ph.D. dissertation, The Ohio State Univ., Columbus, 2001.

[3] E. Rignot, "Mass balance of East Antarctic glaciers and ice shelves from satellite data," *Ann. Glaciol.*, vol. 34, no. 1, pp. 217–227, Jan. 2002.

[4] R. M. Goldstein, H. Engelhardt, B. Kamb, and R. Frolich, "Satellite radar interferometry for monitoring ice sheet motion: Application to an Antarctic ice stream," *Science*, vol. 262, no. 5139, pp. 1525–1530, Dec. 1993.

[5] R. Kwok and M. Fahnestock, "Ice sheet motion and topography from radar interferometry," *IEEE Trans. Geosci. Remote Sens.*, vol. 34, no. 1, pp. 189–199, Jan. 1996.

[6] I. Joughin, "Ice-sheet velocity mapping: A combined interferometric and speckle-tracking approach," *Ann. Glaciol.*, vol. 34, no. 1, pp. 195–201, Jan. 2002.

[7] R. M. Goldstein, H. A. Zebker, and C. L. Werner, "Satellite radar interferometry: Two-dimensional phase unwrapping," *Radio Sci.*, vol. 23, no. 4, pp. 713–720, 1988.

[8] D. Ghiglia and L. Romero, "Robust two-dimensional weighted and unweighted phase unwrapping that uses fast transforms and iterative methods," *J. Opt. Soc. Amer.*, vol. 11, no. 1, pp. 107–117, 1994.

[9] W. Xu and I. Cumming, "A region-growing algorithm for InSAR phase unwrapping," *IEEE Trans. Geosci. Remote Sens.*, vol. 37, no. 1, pp. 124–134, Jan. 1999.

[10] A. Reigber and J. Moreira, "Phase unwrapping by fusion of local and global methods," in *Proc. IGARSS*, Singapore, 1997, pp. 869–871.

[11] R. Bamler and M. Eineder, "Accuracy of differential shift estimation by correlation and split-bandwidth interferometry for wideband and delta-k SAR systems," *IEEE Geosci. Remote Sens. Lett.*, vol. 2, no. 2, pp. 151–155, Apr. 2005.

[12] H. Liu, K. C. Jezek, and B. Li, "Development of Antarctic digital elevation model by integrating cartographic and remotely sensed data: A GIS-based approach," *J. Geophys. Res.*, vol. 104, no. B10, pp. 23 199–23 213, 1999.